arXiv:2611.11402v1 [cs.AR] 8 Nov 2026

A Per-Step Load-Balancing Engine for Expert-Parallel MoE Serving

Jingyuan Li[1], Maolin Wang[2], and Hayden So[1]
[1]The University of Hong Kong
[2]The Hong Kong University of Science and Technology

***Abstract*—In expert-parallel Mixture-of-Experts serving, a layer finishes only when the most loaded GPU of its group does. Token routing shifts at every decode step and concentrates on a few experts, so most of the group's reserved GPU time waits on stragglers. Recovering that time means re-deciding, at every layer of every decode step, how each replicated expert's tokens divide between its copies. The exact linear-program solvers that make this decision optimally take longer than many of the layers they serve, and their working set outgrows GPU shared memory at deployment scale. We introduce Relief, a bidirectional pairwise relaxation that makes the linear program unnecessary, coming within a fraction of a point of the per-step optimum in a few passes of integer halving over the token counts. We build and measure three deployments, CUDA kernels on the serving GPU, the same verified engine on an FPGA over PCIe, and a fixed-function block beside the accelerator. On decode routing from three open MoE families, Relief holds the balance near the per-step optimum at every group size and layer time measured. Scored as effective utilization relative to that optimum, the kernel alone matches or exceeds every deployable scheme at every group size, from the hundred-microsecond layer on. The on-die engine widens that lead at every point, recovering up to 37.3 percentage points over the deployed static placement, while adding 0.02% of a current accelerator's transistors.**

I. Introduction

Mixture-of-Experts models carry a growing share of frontier LLM serving, and expert parallelism is how they deploy. The experts of each MoE layer spread across a group of G GPUs. Every token's hidden state travels to the ranks (the group's member GPUs) that hold its experts, and the layer completes when the most loaded rank finishes [7], [16], [31]. The group therefore runs at the pace of its worst straggler, once per layer, at every decode step.

Token-to-expert assignments concentrate on few experts and shift from step to step. The ranks therefore finish unevenly, and the group's reserved GPU time waits on whichever rank drew the most tokens. The waste is reported wherever MoE serving is measured. Published characterizations place MoE-layer compute utilization below 11% on GPUs [32], while the decode phase draws roughly half of serving's GPU power [26]. On decode routing captured from a 128-expert open model, an unbalanced 64-GPU group performs expert work during a quarter of the GPU time it reserves (§II).

Deployed systems balance today with one static mechanism (Fig. 1). EPLB periodically recomputes which experts are replicated on which GPUs, a placement decision that migrates expert weights and therefore runs minutes apart [5]. Between placements the production engines pick among an expert's replicas by position or at random, oblivious to load. An exact per-step mechanism also exists. LPLB re-solves a min–max linear program over the replica split at every batch on the GPU [6]. Neither mechanism recovers the idle GPU time. The static mechanism cannot track per-step routing, and the distance it leaves to the per-step optimum does not close at any scale (Fig. 4). The exact mechanism fails on its own latency. The counts a per-step split consumes are produced inside the very iteration it serves, so the decision cannot leave the decode loop. The layer dispatches only after the split arrives. For layers near its own $\sim$100 µs solve latency the decision therefore costs more utilization than its balance recovers. Further, its factorization's working set grows with the square of the group against a fixed on-chip capacity, so at deployment scale it stops launching at all (§II-C). Both failures have been read as fundamental. A recent ISCA paper asserts that MoE's dynamism prevents "any load-balancing solutions to better distribute the number of activated experts across the GPUs in an even manner" [12].

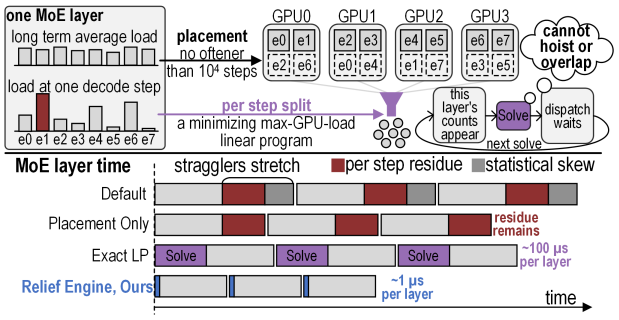


Fig. 1: The per-step balancing problem. Expert load divides into a slow statistical skew, which periodic re-placement absorbs, and a per-step residue, visible only inside the decode iteration, which no deployed mechanism follows. The exact solver follows it and adds $\sim$100 µs to every layer, and the bottom row follows it at this paper's measured silicon latency. Each block of the lower timeline is one MoE layer, and a decode step runs every layer.

The decision-frequency measurement of §II-C contradicts that reading. Reusing a balancing split for even one additional decode step forfeits 62–91.6% of the utilization it recovers over the static baseline, and a free, clairvoyant periodic re-placement collapses to the static baseline as well. No schedule coarser than one decision per step therefore realizes the value a per-step decision holds. That optimum is set by the step's own counts, and the exact solvers reach it at a latency the

layer cannot absorb. Reaching that balance does not require the program. Relief is a bidirectional pairwise relaxation over the placement's replica edges, in integer arithmetic throughout, and a few passes of halving transfers bring the load table to within a fraction of a point of the per-step optimum. Moreover, our best GPU kernels of it already outrun the exact solver, 3.7 to 7.3× call for call, and keep running where the solver cannot launch (§IV-A). What latency remains sits in storage. Every pass re-reads one small table at indices known only at run time, and which storage can hold that table is what separates the deployments of this method (§IV).

We therefore treat deployment as part of the design and build the Relief solve three ways. The kernel runs on one of the serving accelerator's own SMs. The same verified engine runs on an FPGA across PCIe, field-reprogrammable as the deployment evolves. A small fixed-function block sits beside the serving datapath, one per accelerator, of the kind Intel ships for load balancing in Xeon processors [21]. Every deployment consumes the raw per-expert counts in 32-bit fixed point and returns a bit-identical split.

On decode routing from three open MoE families served with expert parallelism at 8 to 64 GPUs, scored as the share of the group's reserved GPU time that performs expert work relative to the best split any policy could produce each step, the deployed placement scheme realizes 66 to 72% of that bound by model family. Our kernel raises the three families to 93%, and our silicon deployment raises them to 99.5%, while adding 0.02% of a modern accelerator's transistors. The largest recovery over the deployed scheme is 37.3 points of that share. At G=64 a fixed ratio on the fitted placement delivers less utilization than no balancing at all, a reversal §II-C traces to the placement's own structure.

This paper makes three contributions.

- **Relief, an all-integer split algorithm that makes the exact solver unnecessary.** A few passes of bidirectional pairwise halving along the placement's replica edges come within a fraction of a point of the per-step optimum, and the working set is the load vector itself.
- **We measure three deployments of the method, from software to silicon.** The kernel outruns the exact solver on the solver's own GPU, and the same verified engine holds the load table in registers on an FPGA across PCIe and as $0.14\,\mathrm{mm}^2$ of silicon beside the accelerator. No deployment is a prerequisite of the method, and the evaluation compares all three under one metric.
- **Effective utilization scores balance jointly with decision latency.** A split loses most of its gain after one step of reuse, so a scheme is only as good as the decision it can repeat every step. We charge each scheme its decision latency against the MoE layer it serves and sweep that layer's duration, covering every interconnect, batch, and GPU generation in one study.

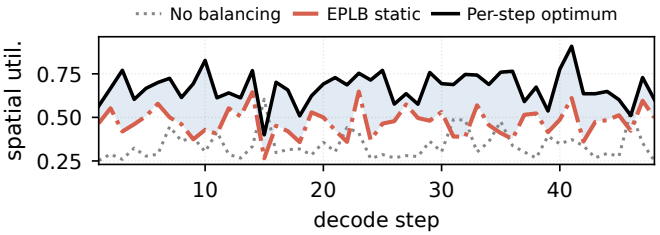


Fig. 2: Per-decode-step spatial utilization, layer 24, G=16. Routing moves every step. A placement fitted to the layer's mean (EPLB static) lifts the trace but tracks none of the motion, while a split re-solved on each step's own counts follows it. The shaded band is what a per-step decision recovers. The optimum stays near 0.67, which is the balance this fixed two-replica placement admits. The remaining distance to 1.0 is set by the placement, which no split can move.

II. Motivation and the Model

A. Expert imbalance leaves provisioned GPU time idle

An expert-parallel MoE layer distributes its experts across a group of G GPUs and completes each decode step at the pace of the most loaded rank. Routing concentrates tokens on few experts, so the ranks finish unevenly. The gap between the mean and the maximum per-rank load is GPU time the deployment provisions and cannot use. On real routing from a 128-expert model (Qwen3-30B-A3B), the spatial utilization of an unbalanced group, the ratio of mean to maximum per-rank load, averages 0.42 at G=16 and falls to 0.24 at G=64 across the model's 48 layers. At deployment scale, three quarters of the provisioned GPU time in the expert stage sits idle behind stragglers, in the regime where fewer than twenty tokens are in flight for 60–70% of machine time [26]. Figure 2 records the volatility itself. On one layer at G=16, routing shifts every decode step. A split frozen from the layer's mean tracks none of the motion, while a split re-solved each step holds the per-step optimum throughout.

In the serving engines that carry production traffic, the per-token choice among an expert's replicas, the *replica pick*, consults no load signal. vLLM resolves a replicated expert by the token position's modulo [15], and SGLang draws the replica uniformly at random [35]. The balancing that deployments do perform operates on a different mechanism and a different timescale. EPLB periodically recomputes which experts are replicated on which GPUs [5], a decision that migrates expert weights between devices and therefore runs no oftener than minutes apart. DeepSeek adjusts its redundant experts every ten minutes when prefilling and states no interval for decoding [7], so thousands of decode steps separate two placements. Between placements the deployed systems hold the split they were given, and the per-step motion of Fig. 2 passes unanswered.

B. The two balancing mechanisms and their timescales

MoE load balancing has two mechanisms, and they differ in what moving them costs. The *placement* mechanism decides which experts, and how many replicas of each, live on which GPU, and moving it copies expert weights across devices.

TABLE I: Balancing mechanisms compared by update rate, use of the current step's loads, per-step decision latency, availability at G=64, and whether the mechanism can reach the per-step optimum at all. §II-C quantifies the latency and the launch limit.

Scheme	Rate	Load-aware	Latency	G=64	Optimum
Replica pick (deployed)	per step	×	∼0	✓	×
EPLB placement (deployed)	minutes	×	0[a]	✓	×
Exact split, software	per step	✓	102 µs	×	✓
Relief (ours, three deployments)	per step	✓	0.75–28 µs	✓	✓[b]

[a] weight migration charged at zero throughout (§V-A). [b] to within a fraction of a point; the fixed point every deployment runs attains 99.5 to 99.8% of it (Table III).

The *split* mechanism decides, for a fixed placement, what fraction of a replicated expert's tokens each replica receives, and moving it rewrites a routing table and moves no weights at all. The imbalance itself divides the same way. One part is a slow statistical skew, the experts that are hot on average, which is what placement absorbs and why a weight-migrating decision need run no oftener than minutes apart, if it runs again at all. The other part is a per-step residue, the deviation of each step's counts from that average, readable only in the step itself. The gating that produces those counts runs inside the decode iteration they serve, so whatever tracks the residue must decide inside that iteration, between the routing that produces the counts and the dispatch that waits on the split (Fig. 1).

The replicated experts form a graph whose edges join the two ranks that hold a copy, and the split chooses one fraction per edge (Fig. 1, top). Everything upstream of the split is already deployed practice, and what the step's counts leave open is the fraction on each edge.

EPLB is deployed and re-decides only the placement. A recent line of exact solvers re-decides the split at every step in software. LPLB re-solves a min–max linear program over the split ratios on the GPU at every batch [6]. No deployed mechanism re-decides the split at every step at a latency the step can absorb. §II-C traces that absence to its cost, and Table I summarizes the mechanisms.

C. Effective utilization and the per-step requirement

The metric follows from GPU-time accounting over one MoE layer at one decode step, the pair every per-step quantity in this paper names. The step's routing scores each token onto k of the layer's E experts and leaves per-expert token counts $n_1, \ldots, n_E$; the placement maps each expert copy to one of the G ranks; and the split divides a replicated expert's count between its two copies. Together the three turn the E per-expert counts into per-rank loads $L_1, \ldots, L_G$, the tokens each GPU serves this step (Eq. 2 below gives L_i in closed form). Each rank then computes for a time proportional to its own load. The layer's synchronous collectives nevertheless hold the whole group until the most loaded rank finishes, so the stage reserves $G \cdot \max_i L_i$ of rank-time to perform $\sum_i L_i$ of expert work. The decision adds latency ahead of the stage. Its input is the counts the iteration just produced, and its output is what the dispatch waits on. It can therefore neither leave the loop nor start early. A solve of latency T_{solve} holds all G ranks that much longer while doing no expert work. Effective utilization is the busy share of everything the group reserves, the product of the balance the split achieves and the share of elapsed time not consumed by the decision,

$$U_{\text{eff}} = \underbrace{\frac{\sum_{i=1}^{G} L_i}{G \max_i L_i}}_{\text{balance: spatial}} \cdot \underbrace{\frac{T_{\text{moe}}}{T_{\text{solve}} + T_{\text{moe}}}}_{\text{share of time executing}} = \frac{\text{spatial}}{1 + T_{\text{solve}}/T_{\text{moe}}}, \tag{1}$$

where T_{moe} is the per-GPU time of everything the layer does once the split is known, the dispatch all-to-all, the expert computation, and the combine all-to-all. The first factor, hereafter spatial, is the mean-to-maximum ratio of per-rank load, and the paper carries the right-hand form. Integrated over a decode trace at a fixed operating point, total useful over total reserved GPU-time is the same expression with the trace's mean spatial in the numerator, and every number in §V is computed exactly so. The paper ranks schemes by this joint quantity.

Every property of a deployment that a balancing scheme does not control enters U_{eff} by moving T_{moe}. The layer time decomposes as $T_{\text{moe}} = T_{\text{disp}} + T_{\text{exp}} + T_{\text{comb}}$. Each all-to-all takes a fixed latency term plus its payload over the link bandwidth, $T_{\text{disp}} \approx \alpha + B\,k\,d_h\,b/(G\,W)$ for batch B, top-k routing, hidden width d_h, and b-byte activations. The expert computation between them scales as B/G on the local GEMM rate. Every such setting enters through one term, so sweeping T_{moe} end to end covers every combination at once. The sweep follows Turbo's methodology [27], and it lets a single-GPU study parameterize a 64-GPU deployment with every group-size-dependent quantity measured at its own G. To place deployments on the range, DeepEP's low-latency decode kernels report the two collective terms alone at 313 µs for 16 ranks and 487 µs for 64, over CX7 RDMA at $W \approx 47$ GB/s [4], before a single expert multiplies, so production decode sits in the upper half of the swept range. A prefill-scale batch raises T_{moe} until any decision latency becomes negligible, and its thousands of tokens smooth the per-step routing itself. The contested region, and this study's traces, are therefore decode. The accounting is conservative, since every scheme's decision is charged as fully blocking. Moreover, the periodic alternatives of §II-C are granted their re-optimization at zero cost, and the split's own communication, a routing table and no expert weights, is inside T_{solve}.

The reference for the numerator is the *per-step optimum*, the best split any policy could produce on the given placement at the given step. It is the solution of an explicit program, the instance of Fig. 1 written in symbols. On a group of G GPUs, rank i carries a fixed load f_i from its non-replicated experts and D replicated slots, two throughout the main study. Slot (i,d) has load $w_{i,d}$ and a second copy on the peer $\sigma(i,d)$ the placement assigns, and $x_{i,d} \in [0,1]$ is the fraction of $w_{i,d}$ that stays on rank i. Rank i's load is then $L_i(x) = f_i + \sum_d w_{i,d}\,x_{i,d} + \sum_{(j,d'):\,\sigma(j,d')=i} w_{j,d'}(1 - x_{j,d'})$, the share it keeps plus the share its peers offload onto it, and balancing

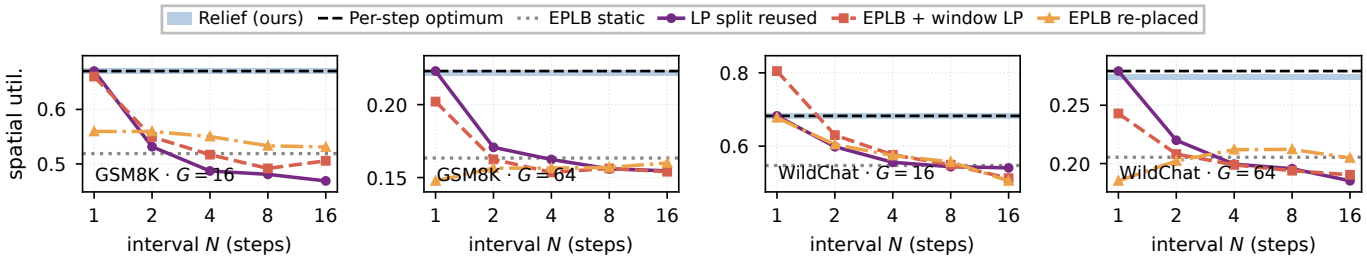


Fig. 3: The per-decision split against periodic balancing on layer 24, both traces and both group sizes, with every periodic scheme's re-solve charged at zero and each window's own future statistics granted. The Relief band coincides with the per-step optimum in every panel, and every periodic scheme leaves it. The one oracle exception (panel c), clairvoyant joint re-fitting at $N{=}1$, migrates expert weights every decode step.

the group minimizes the peak:

$$\min_{x,\,z} \; z \quad \text{s.t.} \quad L_i(x) \le z \;\; \forall i, \qquad 0 \le x_{i,d} \le 1. \tag{2}$$

Total load is conserved across any split, so minimizing the peak z maximizes the mean-to-peak ratio, which is the spatial term of Eq. 1. The program optimizes the very numerator this paper scores against. The exact solvers solve Eq. 2 directly, LPLB with an interior-point method on the GPU [6] and FineMoE on a CPU [34]. The paper takes its solution as the per-step optimum at zero cost and measures every scheme as a distance to this bound. Under Eq. 1 the schemes of §II-B differ only in which factor they give up, as Table I sets out. What remains is to establish at what rate the decision must be made, and what making it costs in software.

Three measurements establish what the missing per-step mechanism requires.

One step of reuse forfeits 62–91.6% of a split's gain. Re-solving every N steps and reusing the split in between avoids the per-step latency. We grant that strategy its best case, a solver re-run on each window's own mean load with the re-solve charged at zero cost, and measure it on real routing (Fig. 3). The reused split falls below the static baseline it was meant to beat by $N{=}4$ in three of the four trace and group-size settings, and by $N{=}8$ in all four. A fitted split tracks the step it was fitted to, while the next step's routing already differs. The same experiment rules out the other alternative. Granted free and clairvoyant re-placement at any interval, with a re-fitted frozen split, the periodic scheme collapses to the static baseline by $N{=}2$ at $G{=}64$ on GSM8K and by $N{=}4$ in two of the three remaining settings. The last, WildChat at $G{=}16$, crosses only at $N{=}16$ and still keeps 61.4% of the per-step gain at $N{=}2$. Weight migration limits the placement to statistics gathered over long windows, and the per-step deviation is visible only to the split. The same limit reaches any placement fitted from window statistics, popularity-proportional replication included [24], since the per-step deviation is not in those statistics. On GSM8K at $G{=}64$ the per-step split wins all 48 layer records at every $N{\ge}2$. The missing mechanism must therefore decide once per layer per decode step, and cheaply.

At that rate, the software solve costs more utilization than its balance recovers. LPLB's solver takes roughly 100 µs per solve on the GPU, a figure its own documentation reports and our measurement confirms at 102 µs. Eq. 1 turns that latency into a utilization loss larger than the balance gain across the range's lower reach. Below $T_{\text{moe}} \approx 103$ µs at $G{=}16$, the exact solver's effective utilization falls under the no-balancing baseline.

At deployment scale the exact GPU solver no longer launches. Equation 2 has $\text{NC}{=}G{+}GD$ load and box constraints for D replicated slots per rank, $3G$ at the two slots per rank the placements use. An interior-point solver factors their $\text{NC}{\times}\text{NC}$ normal-equations matrix once per iteration, and its Cholesky factor occupies $O(\text{NC}^2)$ shared memory, a footprint fixed at compile time by G alone. The solver kernel's own allocation gives it in closed form, $156G^2 + 160G + 40$ bytes on the $D{=}2$ topology family, and that expression reproduces every measured launch footprint exactly. The GPU we measure admits 99 KiB of dynamic shared memory per thread block after opt-in, and the solver stops launching at $G{=}25$, the first size whose footprint exceeds that capacity and the point a launch sweep confirms. The same footprint fits $G{=}32$ inside an A100's 163 KiB and inside the 227 KiB of H100 and Blackwell datacenter parts, so the group size at which the solver stops launching follows the part. At $G{=}64$ the footprint reaches 634 KiB and exceeds the per-thread-block capacity of every current architecture, by $2.8\times$ even against the 227 KiB that H100 and Blackwell datacenter parts offer, the largest opt-in allocation any shipping architecture provides [25].

Figure 4 shows what remains at scale in cost-free balance alone. At $G{=}64$ the fitted placement's fixed ratios measure 0.21 spatial utilization, while the same replica slots under the unfitted default placement measure 0.24, with re-placement and weight migration charged at zero. The per-step optimum, solved on the fitted placement, reaches 0.29. The fitted placement falls below the default because its duplicate map presumes a split that adapts. The planner spreads experts across ranks by their window means and copies each rank's heaviest expert to a fixed neighbour, so the copies of a layer's two heaviest experts share one rank (in every $G{=}64$ layer we probed). Under the deployed replica pick that rank's realized load runs a median $6.8\times$ the median rank's. The same planner fitted to a randomly permuted mean, a placement of identical structure carrying no information about the experts, measures 0.24 and matches the default, which isolates the fit as the source of the loss. Solving the fractions each step on the

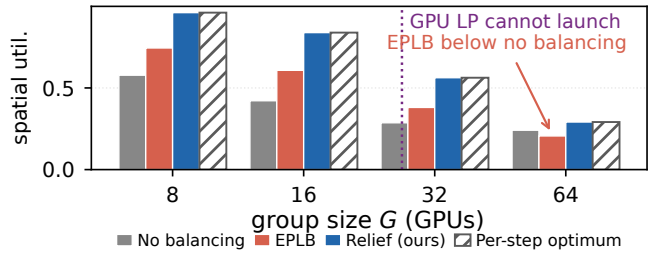


Fig. 4: Spatial utilization by group size on real 128-expert GSM8K routing (layer-major, means of per-layer results), for no balancing, EPLB's static split, the Relief split, and the per-step optimum (hatched). Past the dotted rule the exact GPU solver does not launch on the measured GPU, and at G=64 the static split falls below no balancing. §V-B gives the margins these bars show.

same placement reaches the 0.29, so the fitted placement helps only where a per-step mechanism exists. Without one the deployment does better leaving the default placement in place.

The missing mechanism must therefore return the per-step split at a latency negligible against T_{moe}, at group sizes where the exact GPU solver does not launch. The sections that follow build it.

III. The Relief Algorithm

Balancing on a fixed placement leaves one quantity free. Each replicated expert's tokens divide between its two copies, and that division is one fraction per edge of the replica graph of §II-B. Every choice of fractions is scored by the same live object, the table of per-rank loads for the current step, and flattening this table is the whole objective. The exact solvers reach the fractions through the min–max program of Eq. 2 [6], [34]. Relief edits the table directly (Fig. 5).

A pass visits each transfer in turn and applies the move that is locally most effective for its edge. The move shifts half of the load gap between the transfer's two ranks, and it is truncated to the tokens still available on the sending side. Halving is the amount that levels the two ranks exactly. The cap keeps every fraction inside its range. Because the sign of the gap sets the direction, load flows toward the lighter copy from either side of the edge.

Each move lands in the load table immediately, and the next transfer reads the updated loads. The transfers therefore acquire an order, and a pass becomes a walk of a transfer list against the live table. The convergence depends on that live read, because when every transfer is instead computed from a snapshot taken at the start of the pass, the same balance arrives only after four times the passes (§V-D). A configured number of passes I repeats the walk. Algorithm 1 states one pass, and the procedure is a Gauss–Seidel relaxation of Eq. 2 in integer arithmetic.

A pass walks the transfers one at a time because consecutive transfers may touch the same rank. When they do, the later transfer must read the load written by the earlier one, and any reordering changes the balance the pass reaches. Two transfers that share no rank, however, read and write disjoint entries of

Algorithm 1 One Relief pass, and the emission that follows the last. L is the G-entry load table of Eq. 2; for a transfer t between the two ranks that hold an expert's copies, its home u and its host v, $\text{tok}[t]$ is that expert's token count this step and $\text{mass}[t]$ how many of them are still at u. Every quantity is an integer, and ϵ is one least significant bit.

for each round R of the schedule **do**
  for each transfer $t = (u, v) \in R$, together **do**
    $gap \leftarrow L[u] - L[v]$
    $delta \leftarrow |gap| \gg 1$ {truncating halve}
    $limit \leftarrow gap > 0 \;?\; \text{mass}[t] \;:\; \text{tok}[t] - \text{mass}[t]$ {still at home, or already sent}
    $delta \leftarrow \min(delta, limit)$
    if $delta > \epsilon$ **then**
      $L[u] \mathrel{-}= \text{sgn}(gap)\, delta$; $L[v] \mathrel{+}= \text{sgn}(gap)\, delta$; $\text{mass}[t] \mathrel{-}= \text{sgn}(gap)\, delta$
    end if
  end for
  commit the round; the next round reads what it wrote
end for
after I passes: $\text{o_weight}[t] \leftarrow \text{mass}[t]/\text{tok}[t]$, one reciprocal per replicated expert

the table, so issuing them together produces the same table as issuing them one after the other. The parallelism is therefore discovered inside the serial order, in the way a scheduler finds independent instructions inside a serial program.

Whether two transfers conflict depends only on the ranks named in their edges, and the placement fixes those ranks. The schedule therefore needs no count from any step. Software computes it once, when the placement changes, as a proper edge colouring of the replica graph. Every solve until the next placement walks the same compiled list. The graph has G nodes and GD edges, and its colouring is recomputed only when weight migration moves the placement, minutes apart (§II-B). Every rank touches $2D$ edges, so $2D$ rounds is a lower bound that greedy colouring reaches on every configuration we measure. Further, a $2D$-regular graph coloured in $2D$ colours makes every colour class a perfect matching. Each round therefore holds exactly $\lfloor G/2 \rfloor$ transfers, and the classes tile the list evenly, which is the property behind the fixed-stride issue of §IV-B. The placement hands the solve one list of GD entries in colouring order. Each entry names the two ranks of its transfer and carries no round field, since position alone determines the round.

The last choice inside the algorithm is how many passes to run. Each pass improves the balance, and each pass lengthens T_{solve}, so U_{eff} is a function of the pass count. Substituting the pass count into Eq. 1 and solving for the maximizer states the choice in closed form,

$$I^{*} = \arg\max_{p \le p_{\max}} \frac{s[p]}{1 + \big(L_{\text{if}} + (a + b\,p)\,P\big)/T_{\text{moe}}}, \qquad (3)$$

where $s[p]$ is the balance the relaxation reaches in p passes, measured once for a placement family, and the second term of

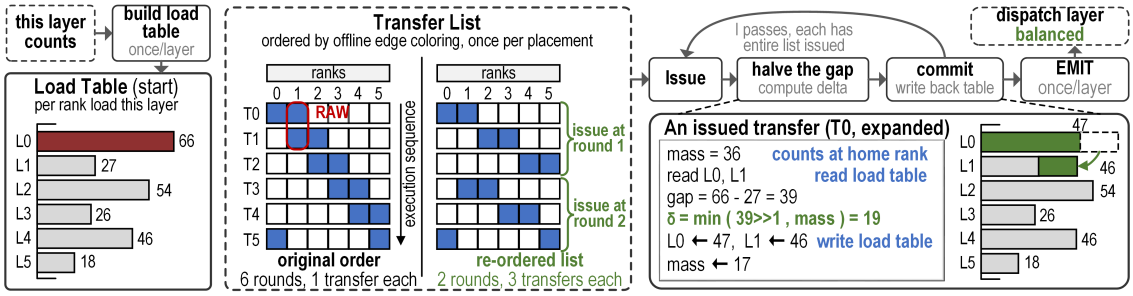


Fig. 5: From counts to emitted fractions. In list order (left matrix) every consecutive pair of the six transfers shares a rank and needs its own round, while the placement-time colouring (right matrix) packs the same six into two rank-disjoint rounds of three. The expanded transfer shows one issue exactly: gap $66 - 27 = 39$, $delta = \min(39 \gg 1, \mathrm{mass}) = 19$, writebacks 47 and 46, the truncated halve leaving the two ranks one apart.

the denominator is the deployment's own T_{solve} at p passes, from its interface latency L_{if}, its cycle model (a, b), and its clock period P. The scan is short, because the balance gained per pass saturates (§V-C). Further, it cannot run inside the solve, because it needs T_{moe}, the duration of the layer being served, and only the driver knows that duration. Balance itself never indicates when to stop, since it improves with every pass. After every pass the load table gives the balance, so one instrumented solve records $s[p]$ for every p at once, and a few such solves at a new placement give the whole curve. The driver therefore evaluates the loop per group size and layer duration once, offline, and writes the result into each call as a plain field, a kernel argument or a descriptor word.

How near the relaxation comes to the per-step optimum is measured in §V-D, in both arithmetics. The fixed-point form every deployment runs is integer addition, comparison, and shift, with one reciprocal at emission. A pass performs $G{\cdot}d$ work in a number of rounds the placement's degree fixes, so group size reaches the algorithm only through the pass count. §V-C measures how that count moves with scale, against an interior-point working set that grows as G^2.

IV. Three Deployments of the Relief Solve

Relief is a fixed-point integer algorithm whose whole working state is one G-entry table and one compiled list, and computation of that shape runs on hardware at every level of a serving stack. This section implements it three ways and measures each one. It runs as a CUDA kernel on the serving GPU, as a silicon block beside the accelerator, and as an FPGA behind PCIe. All three run the same relaxation on the same schedule and return bit-identical splits. They differ in the storage that holds the load table, and therefore in the time a solve takes.

Every deployment leaves the two mechanisms of §II-B on their own clocks, the separation the decision-frequency experiment measured (§II-C). The serving stack keeps the placement it already has, re-fitted at EPLB's own interval, and the split is applied every step on top of it.

A. The Kernel

The kernel runs the whole solve inside one thread block. Shared memory holds the load table and the mass each transfer still keeps at home, and the compiled transfer list arrives as an argument. A pass steps through the list one round at a time. Within a round each lane reads the two loads its transfer names, halves the gap, caps the move by the mass at home, and writes both loads back. The ranks of a round are disjoint, so these writes never collide and the kernel needs no atomic operation. A single barrier separates one round from the next, and it is the only synchronization a pass performs.

Two properties of the algorithm shape this implementation. The round assignment never runs on the device, because it depends on the placement alone (§III), so the device never scores, sorts, or schedules and the list it walks is data. The arithmetic is the engine's own, because a version in the engine's Q11.20 word matches the RTL reference bit for bit at no additional time, so a serving stack that runs the kernel and one that installs the engine obtain the same split. Its own footprint is the G-word load table and the E-entry list, so it launches at every group size, including those past the exact solver's limit (§II-C). §V-B scores what it returns and how quickly.

The transfer list supplies the load table's indices only at run time, and a GPU register file cannot be indexed that way, so the operands live in shared memory. Every dependent step waits on the load-to-use path of roughly 25 ns, with no store-to-load bypass, and caches do not shorten it, since the table always hits and the dependent step then waits the hit latency itself. The kernel needs only the serving GPU a deployment already owns, running on one SM's issue stream.

Every dependent step is a read–modify–write of two load-table entries at run-time indices, and a software implementation performs almost no arithmetic besides it. Solve time therefore tracks the storage that holds the table between dependent steps, and storage is a variable a deployment can choose. The two hardware deployments that follow choose it.

B. Silicon Beside the Accelerator

The second deployment integrates the relaxation as silicon on the accelerator. Every dependent round of the relaxation reads two entries of the G-word load table at indices that the transfer list names and writes them back. In the kernel that table sits in shared memory behind the 25 ns load-to-use path (§IV-A). In silicon the same table is G words of Q11.20 held

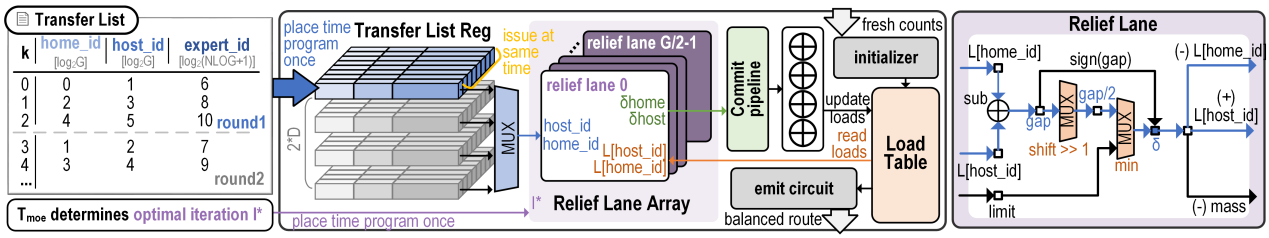


Fig. 6: The engine. The load table is the datapath's only run-time index, and every round both reads and updates it. The transfer list and the pass count I^* (Eq. 3) arrive over the same program-once path. The right panel expands one lane, replicated $G/2$ times.

in registers whose outputs are wires into the arithmetic, so the dependent read takes a wire delay instead of a memory access. The rest of the engine follows from the schedule (Fig. 6). A lane array walks the transfer list, a mass state tracks what each transfer has moved, a reciprocal pipeline emits the fractions, and a descriptor interface connects the engine to the datapath.

The transfer list is the compiled list of §III, entries in colouring order, each naming its *home* rank, *host* rank, and *expert*. A round therefore issues by position alone, every lane's candidates are a compile-time stride of the list, and every transfer of a round issues unconditionally. The one run-time index in the datapath is the load-table read that each entry's rank fields name.

The load table's registers feed the lane array through wires, and a round takes two cycles. The lanes read the two loads each transfer names, halve the gap, and cap it by the transfer's remaining mass (Fig. 6, right). Then the round commits, the per-rank deltas landing at fixed indices. The next round reads what this one wrote, preserving the relaxation's sequential semantics exactly. Mass is tracked as integer tokens, so the loop body holds no division. Once per solve, an eight-lane emit phase converts each transfer's remaining mass to a fraction with one reciprocal, itself precomputed in a two-lane pipeline hidden under the passes. The lane array is sized at $L{=}G/2$ because a colouring round is a perfect matching of exactly $\lfloor G/2 \rfloor$ transfers, so one round fills one issue and a wider array could not issue rounds any sooner. The E-wide scan runs in $\lceil E/L \rceil$ chunks over the same lanes.

On the 128-expert family a solve costs $14{+}8I$ cycles at $G{=}8$ and $28{+}8I$ at $G{=}64$, measured in RTL simulation on the real routing traces. The slope is eight there because that family's topologies colour to their degree lower bound of four rounds and a round costs two cycles, so only the fixed overhead grows with G. Every family's engine is priced on its own measured counts (§V-A), which Table II charges row by row, and each hardware deployment multiplies them by its own clock period. The RTL is bit-exact against the fixed-point reference on 128 of 128 verification programs, so every deployment of the engine computes the same split the kernel does.

The engine sits beside the serving datapath as a bus master, one per accelerator. It consumes the counts that the layer's gating just produced on that die, and it emits the split that the dispatch waits on (§II-C). Every rank routes by the same split, so a centralized decision maker would add a broadcast to that window. LPLB already avoids one by all-reducing the counts and solving the same instance redundantly on every rank [6], and the engine keeps that arrangement. The split is therefore emitted where it is consumed, and the interconnect carries only the counts routing was already exchanging. One engine per die serves every layer of that die, because the relaxation reads the E per-expert counts and runs its measured cycle count regardless of how many tokens the step carries. The engine's duty cycle therefore depends on group size and step rate alone, under 3% of a layer's duration at every operating point of Table II.

The bus interface is a descriptor. Software writes one word naming the count buffer, the pass count, and the result buffer, and rings a doorbell. The engine fetches the raw per-expert counts and derives its internal per-replica view while they arrive, which adds no cycles. It then relaxes and writes the split back. A solve issues only four bus transactions against a slave-port design's 385, a $96\times$ reduction. Charged at a conservative 0.43 µs for the platform's interface latency (the measured mastering path itself takes 0.04 µs), the interface stays a minor term of T_{solve} at every operating point in §V. The mastering logic adds 3.2% to the engine's cell count in synthesis and sits off its critical path.

Each round touches the load vector and the per-replica view, 768 bytes at $G{=}64$, inside a register file of 4.6 KiB in total (Fig. 6).

At the clock-tree stage's 2.89 ns period the relaxation takes 0.36 µs at $G{=}64$ and $I{=}12$. The descriptor interface adds 0.43 µs on top, so at this pass count the bus term exceeds the relaxation at every group size and the interface sets T_{solve}. The engine comes to 0.14 mm^2 of standard cells and ten million transistors (§V-E), and §V-B scores it against every other scheme under Eq. 1.

C. The FPGA Across PCIe

The engine can also be built as a PCIe device. A card added to the host supplies the per-step split to a server already serving MoE models, with no accelerator tape-out. The engine's dimensions are parameters of the RTL (§IV-B), so the card is generated to the group size the server runs. A placement change rewrites the transfer list, and an algorithm change reloads the fabric under the same descriptor contract. Implemented out of context for the XCVH1582 on a VHK158 card, the $G{=}64$ engine routes and closes timing at 7.2 ns, or 139 MHz. Every setup and hold endpoint meets its constraint.

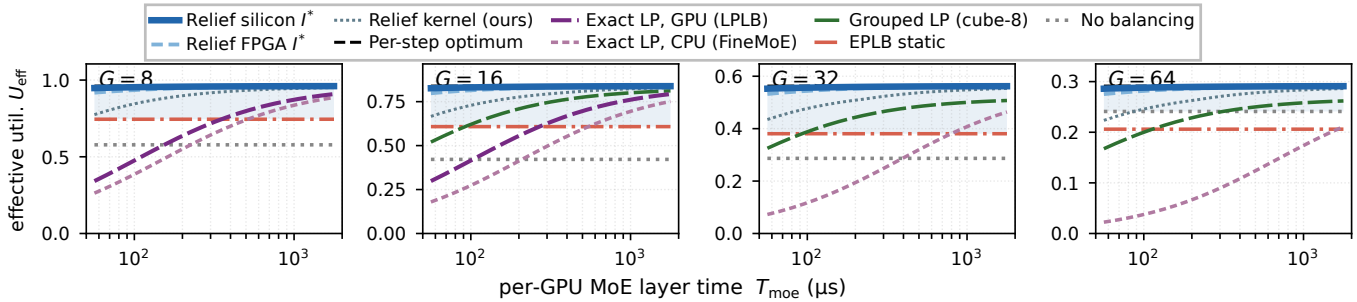


Fig. 7: Effective utilization across the T_{moe} range at every group size, layer-major. The shaded band is what the per-step split recovers over the best static scheme, and each panel carries only the schemes that run at that scale. Production decode layers measure 313–487 µs in their collectives alone (§II-C), in the range's upper half.

The design occupies sixteen percent of the device's LUTs (Table IV). The arrangement differs from the silicon deployment's in one respect. Where each accelerator's engine re-solves the shared instance to keep the answer off the interconnect, the card already sits across a bus. It therefore solves the group's instance once, and the host distributes the returned split. The descriptor and the split cross PCIe, half a kilobyte each way, and the solve is charged a conservative two bus round trips, 2 µs against the literature's ∼0.9 µs per small-payload round trip [23]. T_{solve} comes to 2.9 µs at G=64 and I=12. The card therefore lands between the two other deployments, because the same relaxation runs on a slower fabric clock and crosses a bus that the on-die engine does not. It returns the SM to serving tokens, and §V-B scores it beside the other two.

V. Evaluation

A. Experimental Setup

Routing is captured from three real MoE families on two datasets each, GSM8K and WildChat. Qwen3-30B-A3B (128 experts, top-8, all 48 layers, 48 records per layer) provides the full group-size range, while OLMoE-1B-7B (64 experts, top-8, 16 layers) and Qwen1.5-MoE-A2.7B (60 experts, top-4, 24 layers) repeat the comparison at the group sizes their expert counts admit. Placements are D=2 tori at the power-of-two group sizes deployments use, $G \in \{8, 16, 32, 64\}$ ($C_2 \times C_4$ up to $C_8 \times C_8$), with two replica slots per rank, so a replicated expert lives on exactly two ranks, its home and one peer. An expert count that does not divide G is zero-padded to the next multiple, identically for every scheme. Every balancing scheme runs on the same EPLB placement, computed once from each layer's mean load, and varies only the split. The no-balancing baseline keeps the default placement with the same two redundant slots per rank. The grouped scheme is the deployment LPLB's own documentation recommends at scale. The eight-rank template tiles across $G/8$ independent groups, each solving its own exact program, at a solve latency measured on the same GPU. Every latency in this section is measured on a GPU that admits 99 KiB of dynamic shared memory per thread block after opt-in. The no-balancing and EPLB rows keep the production engines' oblivious replica pick of Table I as their split. Fitting the ratios to the layer mean instead moves the EPLB row in either direction depending on the configuration, so no fixed ratio, tuned or oblivious, responds to the per-step residue. Every number attributed to the engine comes from the fixed-point reference the RTL matches bit-exactly. Every aggregate is layer-major. Each of the 48 layers keeps its own routing ensemble and its own EPLB placement, and cross-layer numbers are means of per-layer results. Pooling records across layers instead fits the placement to an average layer that appears in no trace and counts inter-layer variance as per-step variance, which overstates exactly the adaptation this paper advocates. The reference for every comparison is the per-step optimum, the exact split re-solved every step at zero cost. Each software solver's cost enters through Eq. 1, and its launch limit enters as absence. Producing the placement itself is likewise charged to no scheme, a concession of different size for the two mechanisms. EPLB's re-fit moves expert weights, megabytes per migration, where a placement change costs Relief one recolouring, a 912-byte list written once (§IV-B). Neither charge changes a figure in this section. The engine's cycle counts come from RTL simulation on these traces, at every group size and family, and are the same in every deployment. The silicon deployment's area and timing come from the OpenROAD flow on the ASAP7 7 nm educational PDK [1], quoted from the clock-tree stage, after timing repair, where its analyzer reports a 2.89 ns minimum period with no violated setup or hold path. The parasitics at that stage are global-route estimates. The FPGA deployment is placed and routed to timing closure on its device. Every figure charges the engine as fully blocking, with no overlap with the layer's other work.

B. End-to-End Results

Figure 7 plots U_{eff} across T_{moe} at every group size. The silicon deployment attains the highest effective utilization of any scheme at every point of every panel, and runs within 1% of the cost-free optimum once T_{moe} exceeds a few hundred microseconds. The closing paragraph of this subsection compares the three deployments against one another. Where the exact GPU solver runs, its balance is optimal and its latency still holds it below the no-balancing scheme at the shortest layers. Past its launch limit it has no curve at all (§II-C). The CPU implementation runs at every group size. Its latency keeps it below every per-step alternative, and the same optimum

TABLE II: Effective utilization across schemes, model families, and group sizes. Each cell is U_{eff} as a percentage of the per-step optimum's, with the scheme's measured T_{solve} charged through Eq. 1. Columns nest dataset, operating point (§V-B), then G. Bold marks the best value per column and the shortest T_{solve} per panel. A cross marks a configuration that does not launch on the measured GPU, and at G=64 one whose footprint exceeds every shipping architecture (§II-C). A blank marks a configuration that does not exist. I^* rows re-solve the pass count per operating point. The exact-solver rows repeat across families, each granted the optimum's balance and charged only its latency; a row's mean covers the cells it has. [a]the same placement with the split solved exactly, on the GPU [6] and on a CPU [34]. [b]the grouped solver solves $G/8$ independent eight-rank problems, so both its latency and its balance ceiling belong to that smaller problem. The kernel row's T_{solve} is the latency its caller observes.

	GSM8K									WildChat										
T_{moe} (µs):	100			500			2000			100			500			2000				
Scheme G:	16	32	64	16	32	64	16	32	64	16	32	64	16	32	64	16	32	64	T_{solve}	mean
Qwen3-30B-A3B, 128 experts																				
No balancing	50.3	51.0	82.8	50.3	51.0	82.8	50.3	51.0	82.8	59.6	57.0	77.6	59.6	57.0	77.6	59.6	57.0	77.6		63.0
EPLB (deployed)	72.5	67.7	70.7	72.5	67.7	70.7	72.5	67.7	70.7	77.8	71.0	71.9	77.8	71.0	71.9	77.8	71.0	71.9		71.9
LPLB (GPU LP)[a]	49.5	×	×	83.1	×	×	95.1	×	×	49.5	×	×	83.1	×	×	95.1	×	×	102	75.9
FineMoE (CPU LP)[a]	32.6	20.8	12.9	70.7	56.8	42.5	90.6	84.0	74.7	32.6	20.8	12.9	70.7	56.8	42.5	90.6	84.0	74.7	207–676	54.0
Grouped LP (cube-8)[b]	74.0	69.0	68.7	92.4	86.2	85.9	97.0	90.4	90.1	74.4	68.4	68.8	93.0	85.4	86.0	97.5	89.6	90.3	33[b]	83.7
EPLB + relief (kernel), I^*	86.9	84.8	84.4	96.5	95.5	95.4	99.0	98.6	98.5	87.4	83.0	83.2	96.8	94.7	94.9	99.1	98.3	98.3	13–28	93.1
EPLB + relief (FPGA), I^*	97.1	96.7	96.7	99.3	99.2	99.2	99.8	99.8	99.8	97.2	96.5	96.5	99.4	99.2	99.2	99.8	99.8	99.8	2.8–4.1	98.6
EPLB + relief (silicon), I^*	**99.1**	**98.9**	**98.9**	**99.8**	**99.7**	**99.7**	**99.9**	**99.9**	**99.9**	**99.2**	**98.8**	**98.8**	**99.8**	**99.7**	**99.7**	**99.9**	**99.9**	**99.9**	**0.7–1.7**	**99.5**
G:	16	32		16	32		16	32		16	32		16	32		16	32			
OLMoE-1B-7B, 64 experts																				
No balancing	58.3	66.2		58.3	66.2		58.3	66.2		58.3	68.1		58.3	68.1		58.3	68.1			62.7
EPLB (deployed)	68.8	64.4		68.8	64.4		68.8	64.4		72.6	64.6		72.6	64.6		72.6	64.6			67.6
LPLB (GPU LP)[a]	49.5	×		83.1	×		95.1	×		49.5	×		83.1	×		95.1	×		102	75.9
FineMoE (CPU LP)[a]	32.6	20.8		70.7	56.8		90.6	84.0		32.6	20.8		70.7	56.8		90.6	84.0		207–380	59.3
EPLB + relief (kernel), I^*	86.7	84.4		96.4	95.2		99.0	98.4		87.1	82.9		96.5	94.9		99.1	98.3		13–26	93.2
EPLB + relief (FPGA), I^*	97.0	96.6		99.3	99.1		99.8	99.7		97.2	96.5		99.4	99.2		99.8	99.7		2.8–5.0	98.6
EPLB + relief (silicon), I^*	**99.0**	**98.8**		**99.8**	**99.7**		**99.9**	**99.9**		**99.2**	**98.8**		**99.8**	**99.7**		**99.9**	**99.9**		**0.7–1.6**	**99.5**
Qwen1.5-MoE-A2.7B, 60 experts																				
No balancing	57.5	59.3		57.5	59.3		57.5	59.3		65.1	61.2		65.1	61.2		65.1	61.2			60.8
EPLB (deployed)	68.7	64.0		68.7	64.0		68.7	64.0		70.5	62.6		70.5	62.6		70.5	62.6			66.4
LPLB (GPU LP)[a]	49.5	×		83.1	×		95.1	×		49.5	×		83.1	×		95.1	×		102	75.9
FineMoE (CPU LP)[a]	32.6	20.8		70.7	56.8		90.6	84.0		32.6	20.8		70.7	56.8		90.6	84.0		207–380	59.3
EPLB + relief (kernel), I^*	86.6	83.2		96.3	94.5		98.9	98.0		87.1	84.7		96.5	94.9		99.0	98.2		13–26	93.2
EPLB + relief (FPGA), I^*	97.0	96.3		99.3	99.1		99.8	99.7		97.1	96.4		99.3	99.1		99.8	99.7		2.8–5.0	98.5
EPLB + relief (silicon), I^*	**99.0**	**98.6**		**99.8**	**99.6**		**99.9**	**99.9**		**99.1**	**98.7**		**99.8**	**99.6**		**99.9**	**99.9**		**0.7–2.0**	**99.5**

computed off the GPU never becomes the best scheme in the range.

Table II reports every scheme and model family as U_{eff} relative to the per-step optimum, at three operating points and the group sizes each family admits. They are the exact GPU solver's measured break-even at 100 µs, the 500 µs production decode scale that DeepEP's collectives anchor [4], and a large-batch layer at 2000 µs where decision latency is negligible. Figure 7 carries every point between and beyond them. According to the table, U_{eff} orders the schemes differently than balance does, since the GPU solver holds all of the attainable balance yet delivers less utilization than leaving the split alone at the shortest operating point. The engine's rows are the best deployable value in every column of every family, where the 11.8 to 15.9 points of that share between engine and kernel at 100 µs are the shared-memory path expressed in utilization.

The deployed static scheme's advantage over no balancing changes sign at the largest group. It measures $+16.7$, $+18.6$, $+9.4$, and -3.5 points of spatial utilization across $G \in \{8, 16, 32, 64\}$ on GSM8K, with WildChat replicating the collapse at $+14.8$, $+13.0$, $+7.2$, -1.7, the reversal §II-C isolates with a controlled probe. Relief's per-step split on that same replicated placement reaches 0.28 to 0.29 depending on T_{moe}, five points of balance over the best deployable scheme at the scale where the exact GPU solver does not run at all. The group-local solver is the closest competitor there, and it is the configuration LPLB's documentation recommends for large deployments. Its eight-rank programs solve in a measured 33 µs and never meet the launch limit. They cannot move tokens across group boundaries, so its balance tops out at 91.6% of the optimum's, and the two together leave it at 68.7% at the 100 µs operating point, below the no-balancing row.

At its solved pass counts Relief's balance follows the layer it serves. It stays within 0.17% of the per-step optimum at G=16 and 0.18% at G=64 at the shortest operating point, tightening further from the production scale on. At the production point's pass count it is the best achievable scheme in 190 of 192 layer-group combinations (Fig. 8). On two G=64 layers the default placement with no balancing at all wins by 9 to 12%, because the replicated placement fits that routing worse than the default does. Relief still sits within 0.6% of its own placement's optimum on both layers, so what falls short there is the placement, which remains a separate, composable mechanism (§IV). Figure 8 plots every cell's margin over the best other deployable scheme. The median across all combinations is 19.1 pp and the maximum 31.4 pp. The per-G medians fall

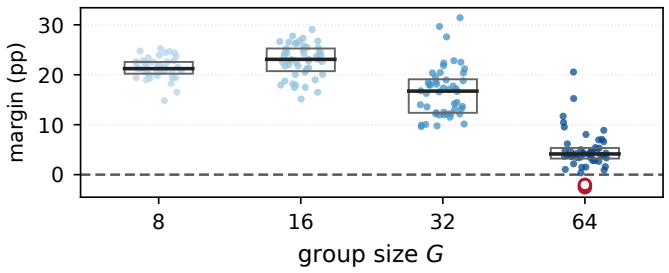


Fig. 8: Spatial-utilization margin of Relief, at the production operating point's solved pass count, over the best other deployable scheme, one dot per layer of the 128-expert family at each group size. Boxes mark quartiles and medians, and the two open red points are the $G{=}64$ exceptions of §V-B. Relief attains the higher utilization in all but those two of the 192 combinations.

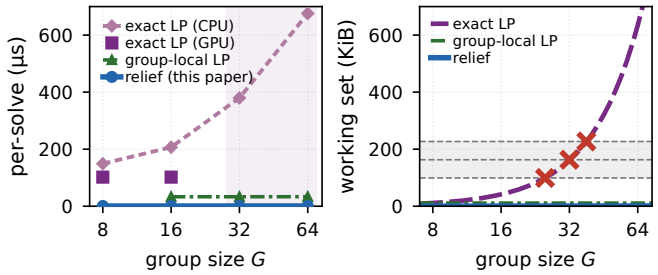


Fig. 9: Per-solve time (left) and working set (right) against group size. The shaded region is where the GPU solver no longer launches on the measured GPU, and each red cross marks where its $156G^2$-byte working set crosses one of the shipping per-thread-block capacities the grey band spans, one cross each for the 5090, A100 and H100. The engine's own curves are flat against both axes.

from the low twenties at $G{\in}\{8, 16\}$ to 4.1 pp at $G{=}64$ as intra-rank pooling thins, and the margin is negative only in the two $G{=}64$ layers above.

Per-solve time is nearly flat in group size (Fig. 9), 0.75 µs at $G{=}8$ to 0.79 at $G{=}64$ for the silicon deployment. The FPGA deployment sits a constant PCIe term above it. The margins therefore persist as the deployment scales. The live working set grows at twelve bytes per rank, where the exact solver's $156G^2$ bytes cross every shipping GPU's shared-memory capacity by $G{=}39$. The expert count enters through the scan schedule alone (§IV-B), so a 256- or 1024-expert model at $G{=}64$ lengthens the scan by a few chunks and changes no wire, port, or register width.

The three deployments differ only in T_{solve}, so every margin between their rows is the interface geometry of §IV.

C. Choosing the Pass Count

The pass count of Eq. 3 follows the layer it serves. I^* spans 6 to 64 across the operating points and group sizes of Table II, because a longer layer absorbs more passes. Both hardware curves of Fig. 7 are drawn at the value it returns. Hardwiring $I{=}12$ instead costs up to 1.6 points of the optimum's share in a cell of Table II, and at most 0.7 of a point on a family mean.

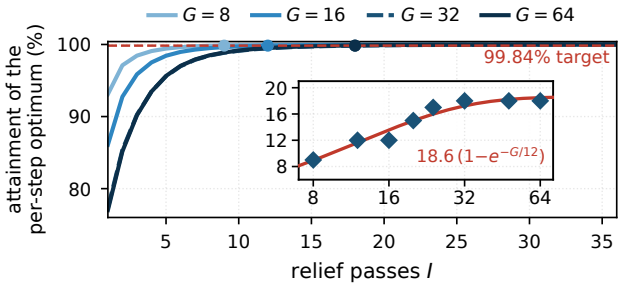


Fig. 10: Attainment of the per-step optimum against pass count, at every integer I from 1 to 36, one curve per group size, with a circle where each curve crosses the 99.84% frontier. The inset gives that frontier's pass count (vertical) against group size (horizontal, diamonds) at eight sizes, the four deployment sizes plus four near-square tori ($G{=}12, 20, 24, 48$) measured only for this scaling. The solid curve there is the saturating fit $18.6\,(1{-}e^{-G/12})$. Three of the eight sizes lie past the measured GPU's launch limit of $G{=}25$.

Over the full (G, I) plane (Fig. 10) the 99.84% attainment frontier, measured at eight group sizes, rises from nine passes to eighteen at $G{=}32$ and stays there.

D. Ablation

Table III compares the relaxation against its own variants and against the rival relaxations, so each difference isolates the removed part. Replacing the live loads with a pass-start snapshot makes the relaxation embarrassingly parallel, a damped Jacobi pass, and removes the most attainment. It loses 4.3 and 9.2 points, recovers Relief's balance only at four times the passes, and diverges without the damping. Among the live-read variants, removing the reverse move loses the most, since flow then only ever leaves the heavier endpoint and a rank made hottest by what it received can never be relieved. The compiled colouring order matches the adaptive walk at $G{=}16$ and lands 0.12 points further at $G{=}64$. Every deployment walks the fixed list that order produces. Water-filling and proportional redistribution, two standard relaxations, land an order of magnitude further from the optimum at an equal pass count. Outside the table, the kernel takes 19–29× longer than the engine for the same splits, the shared-memory path of §IV-A measured at equal pass counts. The descriptor interface's 96× transaction reduction keeps the bus from dominating T_{solve} at Relief's timescale (§IV-B).

The engine computes in Q11.20 fixed point, a 32-bit signed word, the same width as the FP32 solver it displaces, and the lower section of Table III reports every scheme's attainment under each 32-bit arithmetic. Relief's operands are bounded, same-scale integer counts, which a fixed radix point covers exactly, so the fixed word matches the float one. Moreover, the truncating transfer's deadband, by damping the relaxation's small oscillations, even carries the fixed-point split slightly past it at an equal pass count. The narrower rows show the fractional field flat down to 8 bits. The exact LP does not survive the same word, because an interior-point solve is precision-sensitive. Its normal-equations factorization needs the range only a floating radix spans, and in Q11.20 its

TABLE III: Attainment of the per-step optimum under ablations of the relaxation rule and of the arithmetic. Every variant runs at $I{=}12$ passes on the same placement, on the 128-expert family's GSM8K routing, layer-major. FP32 is the exact LP's own precision and produces the reference optimum, so the LP appears only in the fixed-point row.

	attainment of optimum (%)	
Variant	$G{=}16$	$G{=}64$
Relaxation rule		
Relief, engine reference (Q11.20)	**99.84**	**99.51**
without the reverse move	98.80	98.43
snapshot loads, damped (Jacobi)	95.55	90.35
Other relaxations, same pass count		
Water-filling relaxation	86.23	75.22
Proportional relaxation	93.09	81.04
Hash split (deployed)	72.54	70.80
Arithmetic		
relief in FP32 instead	99.68	98.74
relief in Q11.8	99.83	99.49
relief in Q11.4	99.36	99.05
the exact LP in Q11.20	73.68	73.73

TABLE IV: The engine against the dies it would serve, and the FPGA deployment's post-route occupation. Die figures are the vendors'. n/p: not published as a single die. ASAP7 is a predictive 7 nm PDK, less dense than the production nodes, so the area shares are upper bounds and the transistor shares are node-independent.

	absolute		engine share	
Block / accelerator die	mm^2	trans.	by area	by trans.
Relief engine (ASAP7)	**0.14**	**10 M**	—	—
A100 (7 nm)	826	54 B	0.02%	0.02%
H100 (4 nm)	814	80 B	0.02%	0.01%
RTX 5090 (4 nm)	750	92 B	0.02%	0.01%
B200, per die (4 nm)	n/p	104 B	—	0.01%
AMD MI355X, package (3 nm)	n/p	185 B	—	0.01%
Tesla Dojo D1 [29] (7 nm)	645	50 B	0.02%	0.02%
Graphcore GC200 [14] (7 nm)	823	59 B	0.02%	0.02%
	LUTs	FFs	DSPs	BRAM
Relief engine (XCVH1582)	278,895	36,083	20	0

attainment collapses to 73%. The few tenths of a percent that Relief concedes to the optimum change no ranking in §V-B.

E. Hardware Overhead

The engine comes to 0.14 mm^2 of standard cells in a 0.35 mm^2 outline. Its state is 37,434 flip-flops. Its 1.29 M cells are ten million transistors by the per-cell static-CMOS count, 0.005–0.021% of a current accelerator by transistor count and 0.017–0.022% by area, or up to 0.06% if the whole floorplan outline is charged, an order of magnitude below the 0.93% Morpheus reports for its on-die controller [3]. Absolute power is left unreported because vectorless activity estimation diverges on this netlist's reconvergent arithmetic.

VI. Related Work

Exact per-step splitting. LPLB solves the min–max split as an interior-point LP on the GPU [6], and the same formulation balances training micro-batches on CPU solvers [34]; MoETuner casts placement itself as an offline ILP [10]. Our measurements confirm that premise and quantify why software cannot deliver it at decode. Relief reaches the same balance without the program.

Placement and replication. EPLB re-places replicated experts from smoothed statistics [5], and CRAFT allocates replica counts under a memory budget offline [33]. Both decide which expert copies exist, and Relief runs on whatever placement they produce.

Training-time shaping. Auxiliary balance losses [8], [16], loss-free bias adjustment [30], BASE's optimal assignment [17], and expert-choice routing [36] shape the router during training. They set the distribution the serving system receives, while Relief balances, at every step, whatever distribution arrives.

Device-level MoE serving. Accelerator-side work restructures where experts execute. Duplex and MoNDE move low-intensity or cold experts toward memory [13], [32], MoE-OPU compresses and prefetches on one FPGA [22], Pre-gated MoE and ProMoE prefetch predicted experts [12], [28], and SemMoE co-schedules placement with token batching to shrink the all-to-all [19]. A parallel line schedules and overlaps the all-to-all collective itself [11], [18], [20]. They decide where experts execute or how fast tokens travel, and several evaluate under the uniform routing our traces remove, so none of them balances per-step dispatch and all of them compose with a split. Faster collectives in fact raise the weight of the split's latency, since every microsecond removed from T_{moe} increases $T_{\mathrm{solve}}/T_{\mathrm{moe}}$ at any fixed decision cost (Eq. 1).

Hardware load balancers. Balancing at sub-decision-cost granularity has moved into hardware before, for reasons of the same kind. RPCValet steers microsecond RPCs from an on-chip NI because an I/O-bus round trip makes decisions stale [2]; Turbo shows that per-request dispatch keeps its value even against free periodic rebalancing [27]; Intel ships a fixed-function dynamic load balancer on Xeon dies [21]; and AWB-GCN rebalances processing elements inside a sparse accelerator at runtime [9]. The engine balances GPUs in an expert-parallel group, where RPCValet and the Intel block balance cores behind a NIC and AWB-GCN balances lanes inside one accelerator. Re-placement, offline planning, and single-device execution remain the domain of the systems above.

VII. Conclusion

Expert-parallel MoE serving wastes most of its expert-stage GPU time on stragglers, and recovering it takes one balancing decision per layer per decode step, a rate no software solver sustains. Relief comes within a fraction of a point of the per-step optimum in a few passes of integer arithmetic, in a kernel that outruns the solver and in a fixed-function form that adds 0.02% of an accelerator's transistors. Across three model families it matches or exceeds every deployable scheme's effective utilization, recovering up to 37.3 points of that share.

References

[1] L. T. Clark, V. Vashishtha, L. Shifren, A. Gujja, S. Sinha, B. Cline, C. Ramamurthy, and G. Yeric, "ASAP7: A 7-nm finFET predictive

process design kit," *Microelectronics Journal*, vol. 53, pp. 105–115, Jul. 2016.

[2] A. Daglis, M. Sutherland, and B. Falsafi, "RPCValet: NI-Driven Tail-Aware Balancing of µs-Scale RPCs," in *Proceedings of the Twenty-Fourth International Conference on Architectural Support for Programming Languages and Operating Systems*, ser. ASPLOS '19. New York, NY, USA: Association for Computing Machinery, Apr. 2019, pp. 35–48.

[3] S. Darabi, M. Sadrosadati, N. Akbarzadeh, J. Lindegger, M. Hosseini, J. Park, J. Gómez-Luna, O. Mutlu, and H. Sarbazi-Azad, "Morpheus: Extending the Last Level Cache Capacity in GPU Systems Using Idle GPU Core Resources," in *2022 55th IEEE/ACM International Symposium on Microarchitecture (MICRO)*, Oct. 2022, pp. 228–244.

[4] DeepSeek-AI, "DeepEP: An Efficient Expert-Parallel Communication Library," DeepSeek, Jul. 2026.

[5] DeepSeek-AI, "EPLB: Expert Parallelism Load Balancer," DeepSeek, Jul. 2026.

[6] DeepSeek-AI, "LPLB: A Linear-Programming Load Balancer for MoE Expert Parallelism," DeepSeek, Jul. 2026.

[7] DeepSeek-AI, A. Liu, B. Feng, B. Xue, B. Wang, B. Wu, C. Lu, C. Zhao, C. Deng, C. Zhang, C. Ruan, D. Dai, D. Guo, D. Yang, D. Chen, D. Ji, E. Li, F. Lin, F. Dai, F. Luo, G. Hao, G. Chen, G. Li, H. Zhang, H. Bao, H. Xu, H. Wang, H. Zhang, H. Ding, H. Xin, H. Gao, H. Li, H. Qu, J. L. Cai, J. Liang, J. Guo, J. Ni, J. Li, J. Wang, J. Chen, J. Chen, J. Yuan, J. Qiu, J. Li, J. Song, K. Dong, K. Hu, K. Gao, K. Guan, K. Huang, K. Yu, L. Wang, L. Zhang, L. Xu, L. Xia, L. Zhao, L. Wang, L. Zhang, M. Li, M. Wang, M. Zhang, M. Zhang, M. Tang, M. Li, N. Tian, P. Huang, P. Wang, P. Zhang, Q. Wang, Q. Zhu, Q. Chen, Q. Du, R. J. Chen, R. L. Jin, R. Ge, R. Zhang, R. Pan, R. Wang, R. Xu, R. Zhang, R. Chen, S. S. Li, S. Lu, S. Zhou, S. Chen, S. Wu, S. Ye, S. Ye, S. Ma, S. Wang, S. Zhou, S. Yu, S. Zhou, S. Pan, T. Wang, T. Yun, T. Pei, T. Sun, W. L. Xiao, W. Zeng, W. Zhao, W. An, W. Liu, W. Liang, W. Gao, W. Yu, W. Zhang, X. Q. Li, X. Jin, X. Wang, X. Bi, X. Liu, X. Wang, X. Shen, X. Chen, X. Zhang, X. Chen, X. Nie, X. Sun, X. Wang, X. Cheng, X. Liu, X. Xie, X. Liu, X. Yu, X. Song, X. Shan, X. Zhou, X. Yang, X. Li, X. Su, X. Lin, Y. K. Li, Y. Q. Wang, Y. X. Wei, Y. X. Zhu, Y. Zhang, Y. Xu, Y. Xu, Y. Huang, Y. Li, Y. Zhao, Y. Sun, Y. Li, Y. Wang, Y. Yu, Y. Zheng, Y. Zhang, Y. Shi, Y. Xiong, Y. He, Y. Tang, Y. Piao, Y. Wang, Y. Tan, Y. Ma, Y. Liu, Y. Guo, Y. Wu, Y. Ou, Y. Zhu, Y. Wang, Y. Gong, Y. Zou, Y. He, Y. Zha, Y. Xiong, Y. Ma, Y. Yan, Y. Luo, Y. You, Y. Liu, Y. Zhou, Z. F. Wu, Z. Z. Ren, Z. Ren, Z. Sha, Z. Fu, Z. Xu, Z. Huang, Z. Zhang, Z. Xie, Z. Zhang, Z. Hao, Z. Gou, Z. Ma, Z. Yan, Z. Shao, Z. Xu, Z. Wu, Z. Zhang, Z. Li, Z. Gu, Z. Zhu, Z. Liu, Z. Li, Z. Xie, Z. Song, Z. Gao, and Z. Pan, "DeepSeek-V3 Technical Report," Feb. 2025.

[8] W. Fedus, B. Zoph, and N. Shazeer, "Switch Transformers: Scaling to Trillion Parameter Models with Simple and Efficient Sparsity," Jun. 2022.

[9] T. Geng, A. Li, R. Shi, C. Wu, T. Wang, Y. Li, P. Haghi, A. Tumeo, S. Che, S. Reinhardt, and M. Herbordt, "AWB-GCN: A Graph Convolutional Network Accelerator with Runtime Workload Rebalancing," Sep. 2020.

[10] S. Go and D. Mahajan, "MoETuner: Optimized Mixture of Expert Serving with Balanced Expert Placement and Token Routing," Feb. 2025.

[11] C. Hwang, W. Cui, Y. Xiong, Z. Yang, Z. Liu, H. Hu, Z. Wang, R. Salas, J. Jose, P. Ram, J. Chau, P. Cheng, F. Yang, M. Yang, and Y. Xiong, "Tutel: Adaptive Mixture-of-Experts at Scale," Jun. 2023.

[12] R. Hwang, J. Wei, S. Cao, C. Hwang, X. Tang, T. Cao, and M. Yang, "Pre-gated MoE: An Algorithm-System Co-Design for Fast and Scalable Mixture-of-Expert Inference," Apr. 2024.

[13] T. Kim, K. Choi, Y. Cho, J. Cho, H.-J. Lee, and J. Sim, "MoNDE: Mixture of Near-Data Experts for Large-Scale Sparse Models," in *Proceedings of the 61st ACM/IEEE Design Automation Conference*, ser. ACM Conferences, Jun. 2024, pp. 1–6.

[14] S. Knowles, "Graphcore," in *2021 IEEE Hot Chips 33 Symposium (HCS)*, Aug. 2021, pp. 1–25.

[15] W. Kwon, Z. Li, S. Zhuang, Y. Sheng, L. Zheng, C. H. Yu, J. Gonzalez, H. Zhang, and I. Stoica, "Efficient Memory Management for Large Language Model Serving with PagedAttention," in *Proceedings of the 29th Symposium on Operating Systems Principles*, ser. ACM Conferences, Oct. 2023, pp. 611–626.

[16] D. Lepikhin, H. Lee, Y. Xu, D. Chen, O. Firat, Y. Huang, M. Krikun, N. Shazeer, and Z. Chen, "GShard: Scaling Giant Models with Conditional Computation and Automatic Sharding," Jun. 2020.

[17] M. Lewis, S. Bhosale, T. Dettmers, N. Goyal, and L. Zettlemoyer, "BASE Layers: Simplifying Training of Large, Sparse Models," Mar. 2021.

[18] J. Li, Y. Jiang, Y. Zhu, C. Wang, and H. Xu, "Accelerating Distributed MoE Training and Inference with Lina," in *2023 USENIX Annual Technical Conference (USENIX ATC 23)*, 2023, pp. 945–959.

[19] Y. Li, Z. Zhang, Z. Wang, P. Chen, and P. Zheng, "Semantic Parallelism: Redefining Efficient MoE Inference via Model-Data Co-Scheduling," in *International Conference on Learning Representations (ICLR)*, 2026.

[20] J. Liu, J. H. Wang, and Y. Jiang, "Janus: A Unified Distributed Training Framework for Sparse Mixture-of-Experts Models," in *Proceedings of the ACM SIGCOMM 2023 Conference*, ser. ACM Conferences, Sep. 2023, pp. 486–498.

[21] J. Lou, S. Vanavasam, Y. Yuan, R. Wang, and N. S. Kim, "Dynamic Load Balancer in Intel Xeon Scalable Processor: Performance Analyses, Enhancements, and Guidelines," in *Proceedings of the 52nd Annual International Symposium on Computer Architecture*, ser. ISCA '25. New York, NY, USA: Association for Computing Machinery, Jun. 2025, pp. 664–678.

[22] S. Lu, Y. Wei, J. Qian, C. Wu, X. Shi, and L. He, "MoE-OPU: An FPGA Overlay Processor Leveraging Expert Parallelism for MoE-based Large Language Models," in *2025 IEEE/ACM International Conference On Computer Aided Design (ICCAD)*, Oct. 2025, pp. 1–9.

[23] R. Neugebauer, G. Antichi, J. F. Zazo, Y. Audzevich, S. López-Buedo, and A. W. Moore, "Understanding PCIe performance for end host networking," in *Proceedings of the 2018 Conference of the ACM Special Interest Group on Data Communication*, ser. ACM Conferences, Aug. 2018, pp. 327–341.

[24] X. Nie, X. Miao, Z. Wang, Z. Yang, J. Xue, L. Ma, G. Cao, and B. Cui, "FlexMoE: Scaling Large-scale Sparse Pre-trained Model Training via Dynamic Device Placement," *Proceedings of the ACM on Management of Data*, vol. 1, no. 1, pp. 110:1–110:19, May 2023.

[25] NVIDIA, "CUDA C++ Programming Guide (Legacy) — CUDA C++ Programming Guide," https://docs.nvidia.com/cuda/cuda-c-programming-guide/.

[26] P. Patel, E. Choukse, C. Zhang, A. Shah, Í. Goiri, S. Maleki, and R. Bianchini, "Splitwise: Efficient generative LLM inference using phase splitting," May 2024.

[27] H. Seyedroudbari, S. Vanavasam, and A. Daglis, "Turbo: SmartNIC-enabled Dynamic Load Balancing of µs-scale RPCs," in *2023 IEEE International Symposium on High-Performance Computer Architecture (HPCA)*, Feb. 2023, pp. 1045–1058.

[28] X. Song, Z. Zhong, R. Chen, and H. Chen, "ProMoE: Fast MoE-based LLM Serving using Proactive Caching," Sep. 2025.

[29] E. Talpes, D. D. Sarma, D. Williams, S. Arora, T. Kunjan, B. Floering, A. Jalote, C. Hsiong, C. Poorna, V. Samant, J. Sicilia, A. K. Nivarti, R. Ramachandran, T. Fischer, B. Herzberg, B. McGee, G. Venkataramanan, and P. Banon, "The Microarchitecture of DOJO, Tesla's Exa-Scale Computer," *IEEE Micro*, vol. 43, no. 3, pp. 31–39, May 2023.

[30] L. Wang, H. Gao, C. Zhao, X. Sun, and D. Dai, "Auxiliary-Loss-Free Load Balancing Strategy for Mixture-of-Experts," Aug. 2024.

[31] A. Yang, A. Li, B. Yang, B. Zhang, B. Hui, B. Zheng, B. Yu, C. Gao, C. Huang, C. Lv, C. Zheng, D. Liu, F. Zhou, F. Huang, F. Hu, H. Ge, H. Wei, H. Lin, J. Tang, J. Yang, J. Tu, J. Zhang, J. Yang, J. Yang, J. Zhou, J. Zhou, J. Lin, K. Dang, K. Bao, K. Yang, L. Yu, L. Deng, M. Li, M. Xue, M. Li, P. Zhang, P. Wang, Q. Zhu, R. Men, R. Gao, S. Liu, S. Luo, T. Li, T. Tang, W. Yin, X. Ren, X. Wang, X. Zhang, X. Ren, Y. Fan, Y. Su, Y. Zhang, Y. Zhang, Y. Wan, Y. Liu, Z. Wang, Z. Cui, Z. Zhang, Z. Zhou, and Z. Qiu, "Qwen3 Technical Report," May 2025.

[32] S. Yun, K. Kyung, J. Cho, J. Choi, J. Kim, B. Kim, S. Lee, K. Sohn, and J. H. Ahn, "Duplex: A Device for Large Language Models with Mixture of Experts, Grouped Query Attention, and Continuous Batching," in *2024 57th IEEE/ACM International Symposium on Microarchitecture (MICRO)*, Nov. 2024, pp. 1429–1443.

[33] A. Zhao, Z. Cai, Z. Song, L. Yu, H. Fan, J. Wu, Y. Wang, and N. Vijaykumar, "CRAFT: Fine-Grained Cost-Aware Expert Replication For Efficient Mixture-of-Experts Serving," May 2026.

[34] C. Zhao, W. Wu, L. Song, Y. Xu, and Y. Yuan, "Fine-grained MoE Load Balancing with Linear Programming," Jan. 2026.

[35] L. Zheng, L. Yin, Z. Xie, C. Sun, J. Huang, C. H. Yu, S. Cao, C. Kozyrakis, I. Stoica, J. E. Gonzalez, C. Barrett, and Y. Sheng, "SGLang: Efficient Execution of Structured Language Model Programs," Jun. 2024.

[36] Y. Zhou, T. Lei, H. Liu, N. Du, Y. Huang, V. Zhao, A. Dai, Z. Chen, Q. Le, and J. Laudon, "Mixture-of-Experts with Expert Choice Routing," Oct. 2022.

APPENDIX

AI USE

The authors used Claude (Anthropic) to improve the clarity of the paper. All technical content and ideas are the authors' work.